2090 nm 200 W Peak Power 50 ns Pulsed PM Ho-Doped Fiber Amplifier Pumped at 1860 nm

Wiktor Walasik, Robert E. Tench, *Senior Member, IEEE*, Jean-Marc Delavaux, *Senior Member, IEEE*, and Eric Lallier

***Abstract*—We report the design and performance of a 2 μm dual-stage polarization maintaining (PM) holmium-doped fiber amplifier (HDFA) operating in either continuous-wave (CW) or pulsed regime. The amplifier is pumped at 1860 nm, which offers a better efficiency than a 1940 nm pump. In CW regime, we measured more than 1 W of output power at both 2051 nm and 2090 nm signal wavelengths. In pulsed mode, we tested the amplifier over a broad range of pulse widths (50–500 ns) and pulse repetition frequencies (PRFs) (50–1500 kHz). The PM HDFA delivered up to 200 W of peak power and 10 μJ of pulse energy with an excellent stability, while integrated inside a compact module.**

***Index Terms*—Doped fiber amplifiers, infrared fiber optics, optical fiber devices, holmium-doped fiber, polarization maintaining.**

PULSED lasers in the 2000–2150 nm band have generated a lot of interest in medical applications [1], sensing of gases (i.e., CO_2), LIDAR based detection [2]–[5] as well as for pumping optical parametric oscillators and super-continuum sources [6]–[8]. While laser typologies have been successfully demonstrated with both single-mode thulium-doped fibers (TDFs) and holmium-doped fibers (HDFs), the HDF-based lasers have been more intensely studied since their bandwidth of operation allows for efficient emission at wavelengths up to 2150 nm [9]–[12]. High pulse energies of more than 2 mJ as well as record peak powers (10 kW) have been demonstrated with fiber lasers integrating single-clad and double-clad HDFs for pulse widths ranging from nanoseconds to microseconds and pulse repetition frequencies (PRFs) from kHz to MHz [13]–[19].

In this paper, we report the performance of a dual-stage polarization-maintaining (PM) holmium-doped fiber amplifier (HDFA) in both continuous-wave (CW) and pulsed regimes. In our amplifier design, instead of the standard 1940 nm pump, we use a novel in-band pumping wavelength of 1860 nm, which offers better efficiency in commercially available HDFs [20], as it allows to achieve higher population inversion than the same pump power at 1940 nm. In particular, we studied the performance of our HDFA in a master-oscillator power-amplifier (MOPA) arrangement for input signals at the wavelengths of 2051 nm and 2090 nm. In our evaluations, we have compared the HDFA performance for both a narrow (5 MHz) and broad (5 GHz) linewidth laser. For both CW and pulsed modes, we have characterized the performance of both single-stage and dual-stage amplifier configurations. In CW mode, similar Watt-level output powers were demonstrated with either the 5 MHz or 5 GHz laser linewidth at 2051 nm or 2090 nm. In the pulsed mode, we have studied the parametric dependency of the peak power and energy as well as monitored the spectral evolution of the output signal over a broad range of pulse widths (50–500 ns) and PRFs (50–1500 kHz). However, in order to achieve an optimum amplifier performance, we have relied on the 5 GHz laser linewidth at 2090 nm and focused our measurements on a 50 ns long pulse and PRFs of 100 kHz, 200 kHz, and 1 MHz. Overall, we have demonstrated stable and robust pulsed laser performance with more than 200 W of peak power and 10 μJ of pulse energy at 100 kHz PRF. Nevertheless, we have observed that performance was limited by modulation instability (MI) and four-wave mixing (FWM) for low PRF values. Finally, we have shown that our PM HDFA delivers a Watt-level average power with stability better than 5% peak-to-peak variation over a 2 hour period. All the data reported here have been measured with the PM HDFA which has been a fully integrated in a compact module ($200 \times 150 \times 43$ mm^3).

Our manuscript is organized as follows: In Section I, we describe the configuration of the dual-stage PM HDFA and the experimental setup used for its characterization. We report the performance of the first amplifier stage in CW regime in Section II, and in pulse regime in Section III. Next, in Section IV, we investigate in details the performance of the dual-stage amplifier in the CW regime, and in Section V its corresponding pulsed mode performance for a 50 ns pulse width and PRFs of 100 kHz, 200 kHz, and 1 MHz.

I. Experimental Setup

Figure 1 shows the configuration of the PM HDFA. This amplifier consists of a preamplifier stage followed by a booster stage that are separated by a 1 nm bandwidth mid-stage filter centered at the wavelength of 2090 nm. A 6 W 1860 nm pump is split by a 60/40 passive coupler (C1) to counter-pump (40%) the preamplfier stage and co-pump (60%) the booster stage via high-power fiber wavelength division multiplexers WDM1 and WDM2, respectively. We have chosen to use the 1860 nm

Manuscript received March 11, 2021; revised May 14, 2021; accepted May 17, 2021. Date of publication May 19, 2021; date of current version August 2, 2021. *(Corresponding author: Wiktor Walasik.)*

Wiktor Walasik, Robert E. Tench, and Jean-Marc Delavaux are with CYBEL LLC, Bethlehem, PA 18018 USA (e-mail: wiktor.walasik@cybel-llc.com; robert.tench@cybel-llc.com; jm@cybel-llc.com).

Eric Lallier is with Thales Research and Technology, Palaiseau 91767, Cedex, France (e-mail: eric.lallier@thalesgroup.com).

Color versions of one or more figures in this article are available at https://doi.org/10.1109/JLT.2021.3082039.

Digital Object Identifier 10.1109/JLT.2021.3082039

0733-8724 © 2021 IEEE. Personal use is permitted, but republication/redistribution requires IEEE permission.
See https://www.ieee.org/publications/rights/index.html for more information.

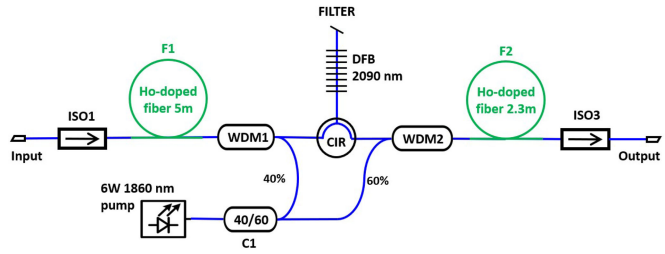

Fig. 1. Schematic of the dual-stage PM HDF pulsed amplifier at 2090 nm.

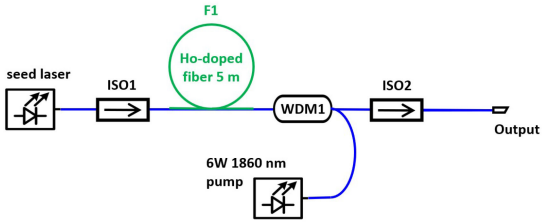

Fig. 2. Schematic of the first stage PM HFDA in CW regime.

wavelength instead of the conventional 1940 nm wavelength in order to achieve optimum optical efficiency between pump and signal in the HDF as recently reported [20]. This behavior is analogous to the effects observed in the Er-doped fiber amplifiers for the two pumping wavelengths of 1480 nm and 1529 nm and a signal band of 1530–1610 nm [21], [22]. The 1860 nm pump is a Tm-doped fiber (i.e., iXblue, IXF-TDF-4-125) linear cavity laser delivering up to 6 W of output power with a spectral width of 0.2 nm and optical signal-to-noise ratio (OSNR) greater than 50 dB/1 nm. Both amplifier stages use the same commercial 8 μm core PM HDF (i.e., iXblue, IXF-HDF-PM-8-125). The fiber gain stage (F1) and power stage (F2) used a 5 m and 2.3 m long PM HDF, respectively. In either CW or pulsed modes, the mid-stage filter removed the out-of-band amplified spontaneous emission (ASE) from the preamplifier stage to saturate the booster. This mid-stage filter was based on an optical circulator (CIR) together with a 1 nm wide 99% reflective fiber Bragg grating (iXblue, IXC-FGB-2090-OPP). The optical insertion loss of the filter was 3.3 dB at 2090 nm.

In our amplifier, for both CW and pulsed mode evaluations, we have used the following PM seed sources: 1) 2 mW single-mode lasers from Eblana Photonics at 2090 nm and 2051 nm, both with the linewidth of 5 MHz; and 2) a 700 mW ring laser at 2090 nm with the linewidth of 5 GHz. The fiber ring laser was built with a 3 m long piece of PM HDF, a filter assembly consisting of a circulator and the same fiber Bragg grating (iXblue-iXC-FGB-2090-OPP) as used in a mid-stage filter of the amplifier described above. The ring laser was pumped with a 3 W 1860 nm fiber laser through a fiber WDM. Additionally a PM isolator was placed inside the ring laser cavity. The fiber output delivered up to 700 mW with a 50 dB/1 nm OSNR and a 5 GHz linewidth via a 60% port of a 60/40 PM coupler.

II. Stage 1 CW

Figure 2 shows the counter-pumped configuration of the preamplifier stage. In this case, an output isolator (ISO2) with a 1 dB loss was used to isolate the gain fiber and the full 6 W of 1860 nm pump was launched into the 5 m of active PM HDF via WDM1, with a 0.8 dB insertion loss. Figure 3 plots the output power (P_{out}) versus pump power at 1860 nm for both 2090 nm and 2051 nm signal wavelength for an input power of 1 mW. For both wavelengths, the output power increases linearly with the pump power and reaches more than 1.1 W of output power or more than 30 dB of signal gain. The slope efficiency is defined as the ratio of signal and pump power increments: $\eta = \Delta P_{\text{out}}/\Delta P_P$. The external optical slope efficiency η is 23.6% and 21.9% for 2090 nm and 2051 nm, respectively. After taking into account the combined loss of 3.1 dB for the WDM1 and ISO2, the internal slope efficiencies η increase to 48% and 45%, respectively. The dashed lines in Figure 3 show the output power obtained with our in-house simulation tool. The simulation is based on the seminal work C. R. Giles and E. Desurvire [23] describing modeling of erbium-doped fiber amplifiers. In our work, the erbium effective gain and absorption profiles have been replaced by those for holmium. The results of the simulations are within 15% and 22% from the experimentally measured values at 2090 nm and 2051 nm, respectively. Contrary to the experiment, the simulations predict somewhat higher output power for the signal wavelength of 2051 nm than for 2090 nm.

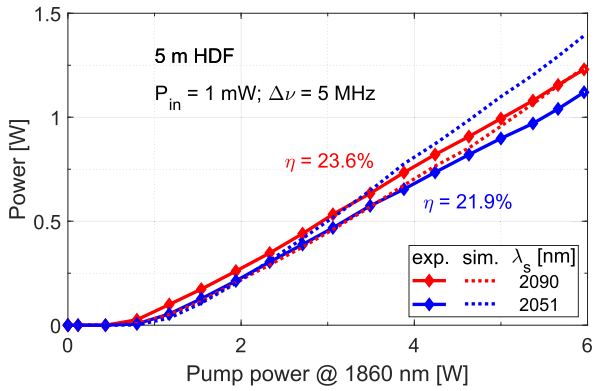

Fig. 3. Output power of the first stage HDFA versus 1860 nm pump power for 1 mW of CW input signals at wavelengths of 2051 nm and 2090 nm.

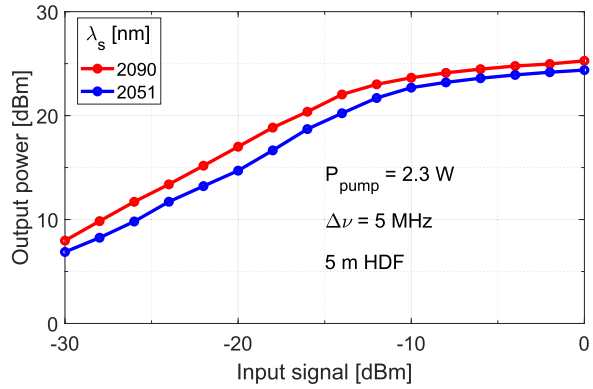

Fig. 4. Output power of the first stage 5 m HDFA versus input signal power for 2051 nm and 2090 nm.

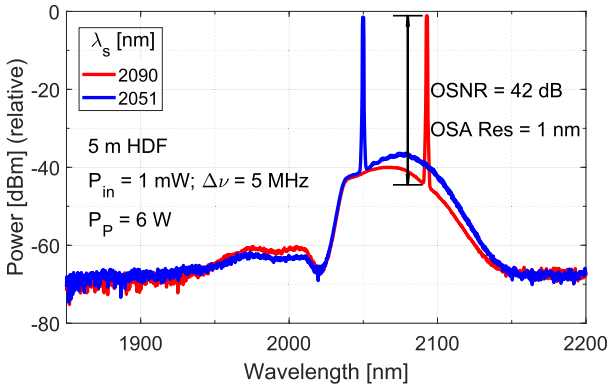

Fig. 5. Output spectra of the first stage PM HDFA for CW input signals at wavelengths of 2051 nm and 2090 nm.

Figure 4 contrasts the output power versus input power for both 2051 nm and 2090 nm. This measurement was performed for 2.3 W of 1860 nm which correspond to 40% of the total 6 W pump available at 1860 nm, which will be used to pump the first stage in our final dual-stage amplifier configuration. The input power is measured after a variable attenuator and before the input isolator. The output performance for both signal wavelengths reveal the same behavior. In the linear regime, the small signal gain is 37 dB and 35 dB at 2090 nm and 2051 nm, respectively. The onset of saturation happens around -12 dBm of input signal, while full saturation occurs for the output power of 25 dBm (i.e., 312 mW) for the input signal above -5 dBm.

The output spectra at $P_P = 6$ W for the two signal wavelengths are shown in Figure 5. The OSNRs measured with respect to the ASE level at the signal wavelengths of 2090 nm and 2051 nm are 42 dB and 39 dB, respectively. The spectra were recorded with 1 nm resolution by the Yokogawa AQ6375 optical spectrum analyzer (OSA). The sharp cut-off of the ASE around the wavelength of 2030 nm is caused by the WDM transmission response. The 10 dB bandwidth of the first stage HDFA, where we would expect to observe a similar performance, is equal to 80 nm and spans from 2030 nm to 2110 nm. This fact is confirmed by our numerical simulations, showing that for $P_P = 6$ W, more then 1 W of output power is expected in the range between 2030 nm to 2110 nm. Further experimental evaluation of the gain bandwidth will be carried out later.

III. Stage 1 Pulsed

Following the characterization of the amplifier stage in a CW regime, we have performed its evaluation for pulse length $\tau = 50$ ns at 2090 nm for three PRFs of 100 kHz, 200 kHz, and 1 MHz. In order to generate the pulse input signal at the wavelength of 2090 nm, we have amplified the signal with an external HDFA, modulated the output of the laser sources using a PM acousto-optic modulator (AOM) and adjusted the average input power of the pulsed signal to 1 mW for each of the three PRF values.

When using the 5 MHz 2090 nm narrow linewidth laser as the seed source to the preamplifier stage, regardless of the PRF setting the pulse peak power was limited to 30 W before

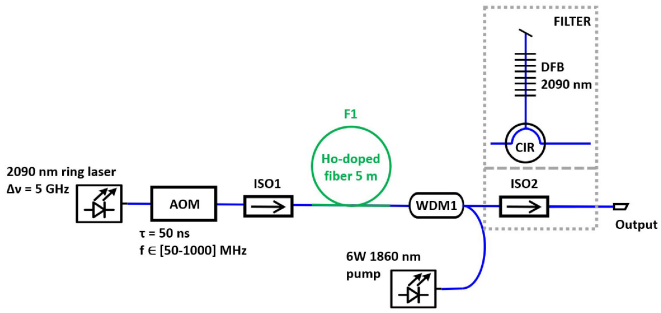

Fig. 6. Schematic of the first stage amplifier in the pulsed regime.

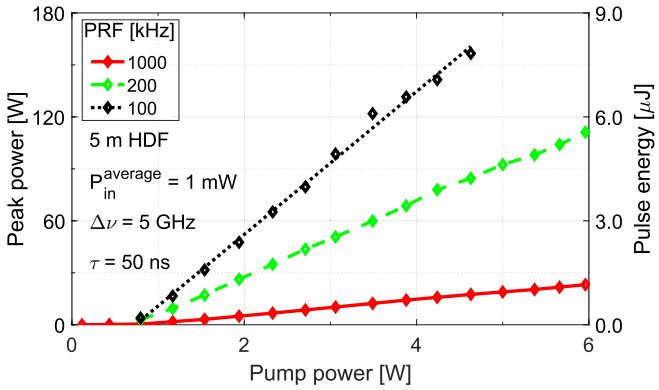

Fig. 7. Peak output power and pulse energy of the first stage PM HDFA versus 1860 nm pump power for input signal composed of 50 ns pulses at PRF of 100 kHz, 200 kHz, and 1 MHz.

generating a nonlinear super-continuum in the fiber [24]. Therefore, we switched to the 2090 nm ring laser which delivers a 5 GHz linewidth and allowed to characterize our pulsed amplifier configuration.

Figure 6 shows the experimental setting used to measure the performance of the preamplifier stage, first with an output isolator, then replaced by the mid-stage filter. In this evaluation, we used the full power (i.e., 6 W) of the 1860 nm pump.

Figure 7 shows the dependence of peak output power and energy for the 5 m HDF amplifier when seeded with 1 mW of average power for 50 ns pulses at three different PRFs. For PRFs of 200 kHz and 1 MHz, we have observed a linear increase of the peak power and energy as a function of the pump power without any major output spectral change. At the maximum pump power of 6 W, the peak power reached 23 W for PRF of 1 MHz and 110 W for PRF of 200 kHz. For the PRF of 100 kHz, the peak power also increased linearly up to the level of 150 W, corresponding to 7.5 μJ for 4.5 W of pump power, and then started exhibiting unstable spectral behavior due to nonlinear phenomena.

Figure 8 illustrates the evolution of the output spectrum as a function of the pump power level for the PRF of 100 kHz. For low pump power, the OSNR is limited predominantly by the ASE from the HDF. As the pump power increased above 3.5 W, MI side bands on both sides of the base band signal appeared and the ASE power broadened towards longer wavelengths due to FWM. These observations are typically associated with MI [16], [19], [25].

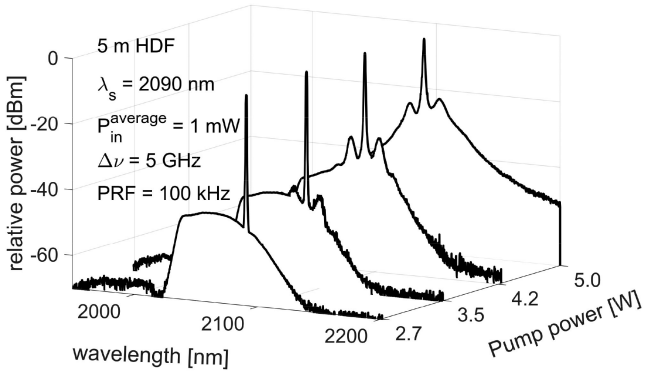

Fig. 8. Evolution of the output spectrum with the 1860 nm pump power for 50 ns long pulses at the PRF of 100 kHz.

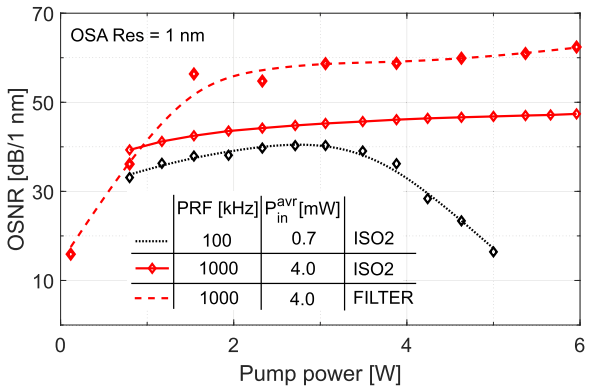

Fig. 9. Dependence of the OSNR of the output signal on the 1860 nm pump power for PRFs of 100 kHz and 1 MHz. At PRF of 1 MHz, the OSNR measured with the output isolator ISO2 and filter are compared.

The dependence of the OSNR of pulsed signal on the pump power is shown in Figure 9 for both PRFs of 100 kHz and 1 MHz. The OSNR for the PRF of 100 kHz reaches 40 dB at 1 nm resolution for 3 W of pump power and then decreases down to 17 dB/1 nm at 5 W of pump power. The degradation of the OSNR for the PRF of 100 kHz at pump powers above 3 W is a direct consequence of the increased level of the ASE seen in the spectra shown in Figure 8. Therefore, in order to ensure that the first stage operates free of nonlinear effects, the pump power to the first stage is limited to the level of 2.4 W, which explains our choice of the 60/40 power splitter C1. Our simulations have shown that the optimal splitting ratio for the splitter C1 is 80/20. However, our choice of 60/40 splitter, leads only to 15% decrease in the output power. In contrast, for the PRF of 1 MHz, the OSNR remains higher than 40 dB/1 nm for pump powers above 1 W and reaches 47 dB/1 nm for the maximum pump power of 6 W.

Next, in order to improve the OSNR and remove the ASE power, we have replaced the isolator (ISO2) by the mid-stage filter centered at 2090 nm. Figure 10 compares the output spectrum of the amplifier at PRF of 1 MHz with an output isolator and with the mid-stage filter output. It is clear that the use of the filter allows us to eliminate the ASE power without attenuating significantly the output power (filter attenuation is 2 dB larger than that of the isolator).

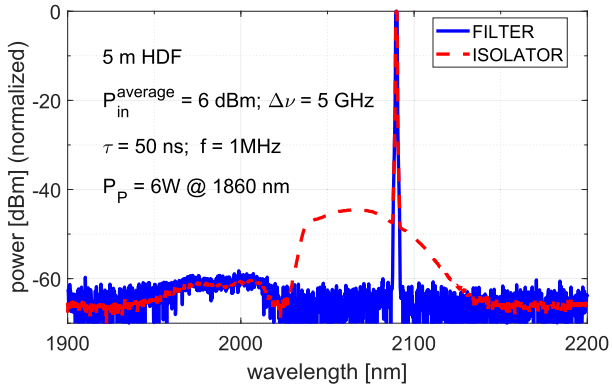

Fig. 10. Output spectra from the first stage with output isolator (red) and output filter (blue).

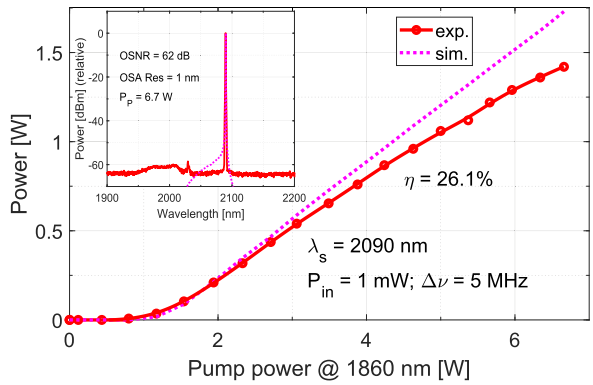

Fig. 11. CW output power of the dual-stage HDFA versus 1860 nm pump power.

In Figure 9, we have plotted the OSNR of the preamplifier output with the filter in place as a function of the pump power for the PRF of 1 MHz. The OSNR remains above the level of 54 dB/1 nm for the pump power above 1.5 W and reaches up to 62 dB/1 nm at $P_P = 6$ W.

IV. Dual-Stage CW

The schematic of the dual-stage HDFA is shown in Fig. 1. Prior to considering its CW performance, the second-stage amplifier was tested separately with a CW signal in a co- and counter-pumped configurations with up to 4 W of 1860 nm pump power. Ultimately, we have adopted the co-pumped arrangement for the 2.3 m long HDFA, since, in saturation, it provided a better efficiency (of more than 15%) with negligible pump throughput.

Figure 11 shows the linear dependence of the output power of the dual-stage HDFA on pump power for 1 mW of CW input at 2090 nm. The maximum power of the amplifier reached 1.4 W for 6.7 W of pump power, leading to a slope efficiency of 26% and a gain of 31.4 dB. Taking into account the 0.9 dB insertion loss of the output isolator, the internal optical efficiency increases to 32%. The dashed line in Figure 11 represents the result of simulations for the dual-stage amplifier. The agreement is relatively good with a slight departure from linearity of the experimentally measured values leading to the slope being 18% smaller than that observed in the simulations. This discrepancy

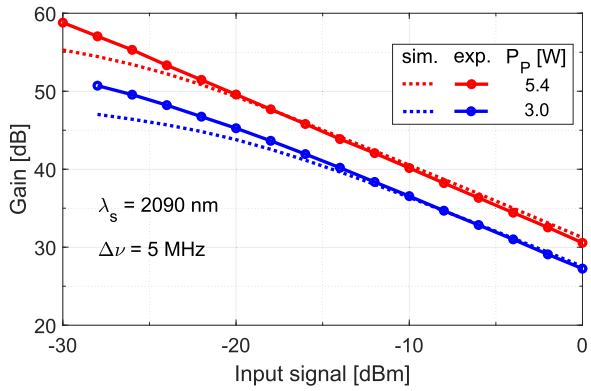

Fig. 12. Gain of the dual-stage PM HDFA versus input signal power at 2090 nm.

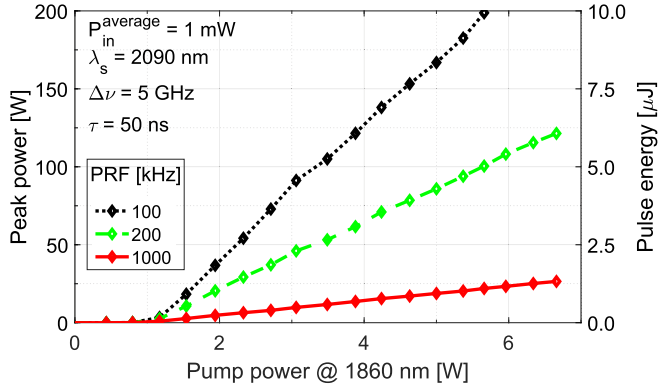

Fig. 13. Peak output power and pulse energy of the dual-stage PM HDFA versus 1860 nm pump power at PRF of 100 kHz, 200 kHz, and 1 MHz.

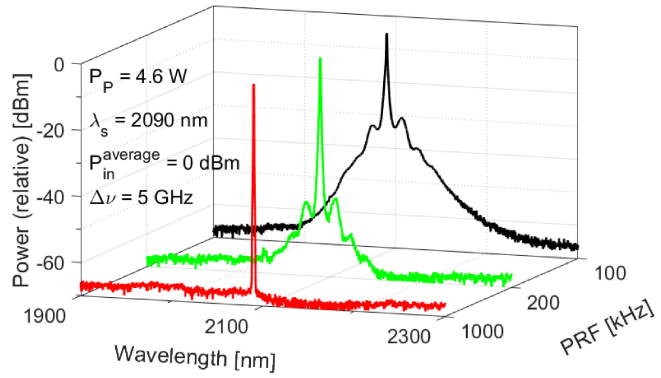

Fig. 14. Comparison of the output spectra of the dual-stage PM HDFA for the PRFs of 100 kHz, 200 kHz, and 1 MHz.

might be caused by the fact, that our simulation tool does not take into account effects related to excited state absorption. As shown in Ref. [26], at high powers, the excited state absorption contributes to a non-linear, pump-dependent loss of signal power. The inset of Figure 11 shows a typical CW spectrum of the HDFA measured at $P_{\text{out}} = 1.4$ W with an OSNR of 62 dB/1 nm. The simulated spectrum is also shown and is a good match to the experimental spectrum. The large OSNR value resulted from the use of the mid-stage filter, which also limited the residual ASE outside of the signal base band. However, one consequence of the co-pumped arrangement was the presence of the unabsorbed pump at the output of the amplifier. The maximum residual 1860 nm pump power throughput was 20 dB below the 2090 nm signal power and could be filtered-out with a narrow-band filter.

In Figure 12, we plotted the gain of the dual-stage HDFA against the input signal for both 3 W and 5.4 W of 1860 nm pump power. For both levels of pump power, the HDFA gain is linear with respect to the input signal, and indicates more than 30 dB of small-signal gain per amplifier stage. In addition, we measure the signal dynamic range of 30 dB (i.e., from -30 dBm to 0 dBm). The net gain of 60 dB, which include both input and output isolator insertion losses (i.e., $0.9 + 1.2$ dB), have been measured at 2090 nm. Although, based on our numerical simulations a similar amplifier performance for the 2030 nm to 2100 nm bandwidth is expected, it needs to be experimentally confirmed. The agreement between the simulations and experiment is very good, in particular for the input signal powers above -15 dBm. At low input signal levels, the simulations slightly underestimate the values measured experimentally.

V. Dual-Stage Pulsed

Next, we have studied the performance of the dual-stage HDFA in the pulsed regime. Figure 13 shows the dependence of the peak power and pulse energy versus total 1860 nm pump power for 50 ns pulses with a constant input average power of 1 mW for PRFs of 100 kHz, 200 kHz, and 1 MHz. For the 1 MHz and 200 kHz, the peak power increases linearly with the pump power, and reaches 26 W and 120 W at the maximum pump power of 6.7 W, respectively. In contrast, for the 100 kHz PRF, the peak power yield a quasi-linear dependence and we have observed a slope change at around 3 W of pump power. Nonetheless, the peak power reaches 200 W corresponding to a pulse energy of 10 μJ for 5.7 W of pump power. This slope change is caused by the onset of the nonlinear effects leading to the spectral broadening of the signal, generation of side lobes due to modulation instability, and pronounced ASE wings as illustrated in Figure 14.

In Figure 14, we compare the typical spectra measured for the three different PRFs for 4.6 W pump power and the average input signal power of 1 mW at 2090 nm. For the PRF of 1 MHz, the output spectrum, represented by the red curve, resembles the spectrum measured for CW operation and features an OSNR of 63 dB/1 nm. The spectrum remains unchanged for the maximum pump power. For the PRF of 200 kHz, the output signal spectrum, shown in green, exhibited a clear spectral broadening. Indeed with the increase of pump power, the laser spectrum broadens and develops side-bands on both sides of the signal wavelength, leading to the decrease in OSNR. We measured an OSNR of 58 dB/1 nm up to a pump power of 3.5 W, which then decreased to 30 dB/1 nm for 6.7 W of pump power. For the PRF of 100 kHz, the laser spectrum is significantly broadened by the nonlinear effects which are clearly visible as illustrated by the black curve. This spectral broadening starts at even lower pump power and increases for higher pump power. We measured an OSNR of 52 dB/1 nm for 2.7 W of the pump power, which decreases to 25 dB/1 nm for the maximum pump power. Similar observations

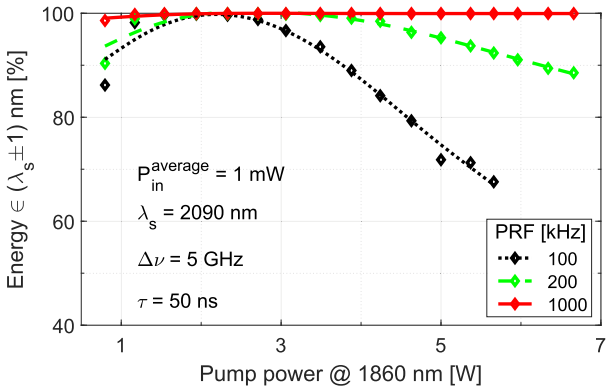

Fig. 15. Fraction of energy contained in within a ±1-nm-wide band centered at the signal wavelength for the dual-stage HDFA versus 1860 nm pump power at PRF of 100 kHz, 200 kHz, and 1 MHz. Points represent the experimental measurements while lines show best fits.

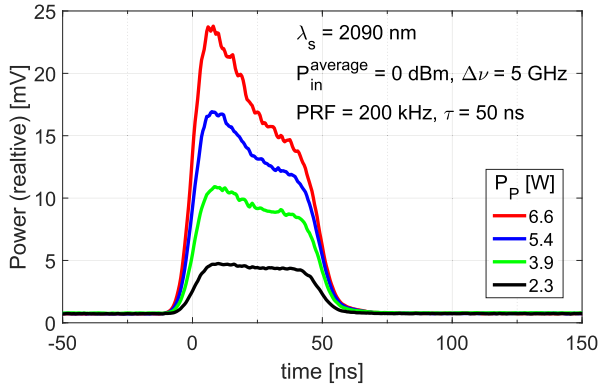

Fig. 16. Evolution of the output pulse shape of the HDFA with the increase of the pump power.

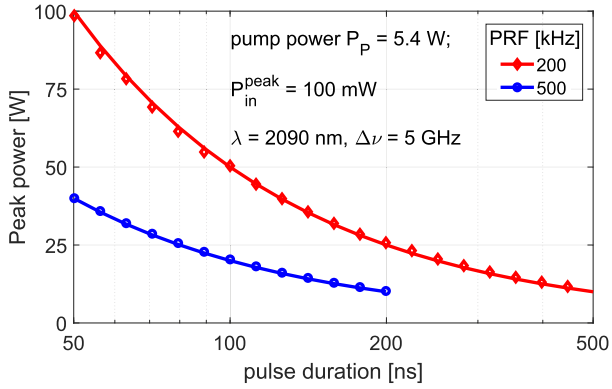

Fig. 17. Peak output power of the dual-stage PM HDFA versus input pulse width for the PRFs of 200 kHz and 500 kHz.

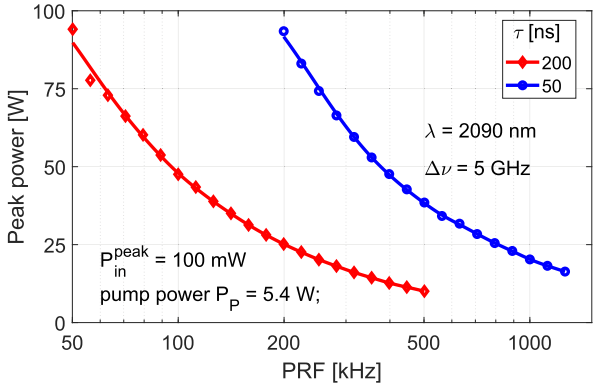

Fig. 18. Peak output power of the dual-stage PM HDFA versus PRF for the pulse duration of 50 ns and 200 ns.

of a spectral broadening have been reported for amplification in pulsed PM HDFA at the 2090 nm wavelength [16], [19]. One way to mitigate such a spectral broadening would be to use a fiber with larger core [14].

Figure 15 shows the dependence of the fraction of the energy in the signal band versus 1860 nm pump power for the dual-stage PM HDFA operating at PRFs of 100 kHz, 200 kHz, and 1 MHz. This energy fraction $\xi_{1\ \mathrm{nm}}$ is defined as a ratio of the energy contained within the ±1-nm-wide band $E_{\pm 1\mathrm{nm}}$ centered at the signal wavelength to the total energy E_{tot} (for wavelengths between 1900 nm and 2300 nm), i.e., $\xi_{1\ \mathrm{nm}} = E_{\pm 1\mathrm{nm}}/E_{\mathrm{tot}}$. For the PRF of 1 MHz, $\xi_{1\ \mathrm{nm}} > 99\%$ for the entire range of used pump power, P_P. However, for the PRF of 200 kHz, $\xi_{1\ \mathrm{nm}}$ remains above 95% for P_P from 1 W to 5 W and drops to the level of 89% for the maximum pump power as a result of the spectral broadening of the signal. Finally, for the PRF of 100 kHz, $\xi_{1\ \mathrm{nm}}$ decreases for the pump power higher than 2.5 W and reaches 68% for $P_P = 6.7$ W. This decrease is caused, in addition to the signal broadening, by the increase of the ASE level. For comparison, at PRF of 100 kHz and $P_P = 6.7$ W, more than 78% (82%) of the total output energy is contained within the bandwidth of ±2 nm (±5 nm) around the signal wavelength. Assuming that the remaining energy is contributed by the ASE, allows us to conclude that the ASE constitutes around 20% of the total output power.

Following our studies of the amplifier output spectra, we consider the typical pulse shape evolution versus output power. Figure 16 illustrates the pulse shape change measured at the several output power levels for a PRF of 200 kHz. The input pulse shape from the acousto-optic modulator was a quasi-rectangular pulse with full-width half-maximum (FWHM) of 50 ns and a 10 ns rise and fall times. At pump power below 3 W, the pulse shape remains unchanged by the HDFA while for higher pump powers, up to 6 W, gain peaking becomes more visible and the pulse shape is deformed into a trapezoidal shape with strong leading edge. Such pulse distortion can be corrected by preshaping the input pulse [27]–[30].

Next, in Figs. 17 and 18, we demonstrate the versatility of our PM HDFA, by measuring the output peak power for a range of pulse widths and PRFs. In particular, Figure 17 shows the dependence of the peak output power as a function of the pulse duration for PRFs of 200 kHz and 500 kHz. The measured data points (i.e., diamonds or circles) follow the fits corresponding to pulse energies of 5 μJ and 2 μJ, for the PRFs of 200 kHz and 500 kHz, respectively.

In Figure 18, we plotted the dependence of the peak output power of the HDFA on PRF for the pulse lengths of 50 ns and 200 ns. It is worth noting that for a 200-ns-pulse at the PRF of 50 kHz, the peak power reached 94 W leading to the pulse energy

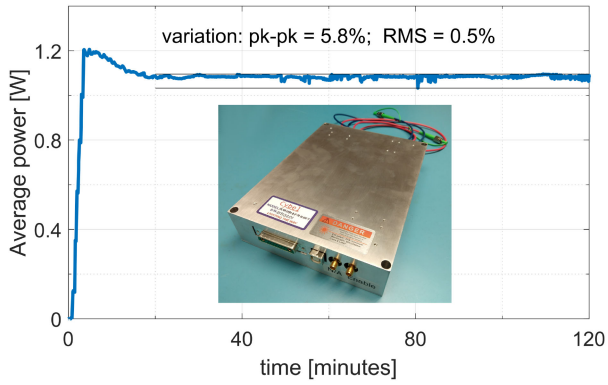

Fig. 19. Stability of the output power of the dual-stage PM HDFA over the period of 2 hours. The inset shows the photo of the $200 \times 150 \times 40$ mm^3 PM HDFA module.

of 18.8 μJ, after the optical output isolator with the loss of 1.2 dB. Overall, all these parametric measurements demonstrate that our pulsed PM HDFA delivers a robust and stable performance. In fact, all our reported performance results were achieved in a fully integrated PM HDFA.

The inset of Figure 19 shows a photograph of the pulsed PM HDFA module, which has dimensions of $200 \times 150 \times 41$ mm^3. It incorporates full pump-control electronics, and communicates via a serial interface. The mass of the packaged amplifier including fiber pigtails and connectors is less than 1 kg. In Figure 19, we have plotted the power stability of the pulsed HDFA as a function of time for 5.4 W of pump power and a 1 mW average input power at a PRF of 200 kHz. After 20 minutes of warm-up time, the HDFA delivered a stable 1.1 W of output power over a 2 hour operation. The measured peak-to-peak (pk-pk) power variation was 5.8%, while the root mean square variation (RMS) was at the level of 0.5%. During the stability measurements, the HDFA was enclosed in a compact module and was mounted on a heat sink cooled by forced airflow.

VI. Conclusions

We have reported the performance of a dual-stage PM holmium-doped fiber amplifier in a MOPA arrangement at the operating wavelengths of 2090 nm and 2051 nm. We have presented both CW and pulsed results for single-stage and dual-stage amplifier configuration using a 1860 nm pump wavelength. This novel scheme for pumping holmium-doped fibers at 1860 nm has been shown to be more efficient than the traditional 1940 nm pump wavelength as confirmed in all our reported pulsed measurements. In the CW mode, the single-stage and dual-stage fiber amplifiers deliver more than 30 dB of small signal gain per stage and an output power greater than a 1 W for 5 W of pump power together with an OSNR greater than 50 dB/1 nm. In the pulsed mode, our parametric evaluation of the single-stage and dual-stage configurations reveals stable and robust peak power and energy for a 50 ns pulse width for 100 kHz, 200 kHz, and 1 MHz pulse repetition frequencies. For the single-stage (dual-stage) amplifier, the peak power and energy at 100 kHz were 150 W (200 W) and 7.5 μJ (10 μJ), while the corresponding OSNR was 34 dB/1 nm (25 dB/1 nm). All our reported performance results were achieved in a fully integrated and packaged PM HDFA. Our amplifier module ($200 \times 150 \times 43$ mm^3) delivers a 1.1 W/CW and 100 W/pulse power with a stability better than 5% over a 2 hour period. The similar HDFA performance are anticipated over the bandwidth from 2030 nm to 2100 nm.

References

[1] N. S. Nishioka and Y. Domankevitz, "Comparison of tissue ablation with pulsed holmium and thulium lasers," *IEEE J. Quantum Electron.*, vol. 26, no. 12, pp. 2271–2275, Dec. 1990.

[2] T. J. Wagener, N. Demma, J. D. Kmetec, and T. S. Kubo, "2 µm LIDAR for laser-based remote sensing: Flight demonstration and application survey," *IEEE Aerosp. Electron. Syst. Mag.*, vol. 10, no. 2, pp. 23–28, Feb. 1995.

[3] F. Gibert, P. H. Flamant, D. Bruneau, and C. Loth, "Two-micrometer heterodyne differential absorption lidar measurements of the atmospheric CO_2 mixing ratio in the boundary layer," *Appl. Opt.*, vol. 45, no. 18, pp. 4448–4458, 2006.

[4] S. Ishii *et al.*, "Coherent 2 µm differential absorption and wind lidar with conductively cooled laser and two-axis scanning device," *Appl. Opt.*, vol. 49, no. 10, pp. 1809–1817, 2010.

[5] G. D. Spiers *et al.*, "Atmospheric CO_2 measurements with a 2 µm airborne laser absorption spectrometer employing coherent detection," *Appl. Opt.*, vol. 50, no. 14, pp. 2098–2111, 2011.

[6] N. Leindecker *et al.*, "Octave-spanning ultrafast OPO with 2.6-6.1 µm instantaneous bandwidth pumped by femtosecond Tm-fiber laser," *Opt. Exp.*, vol. 20, no. 7, pp. 7046–7053, 2012.

[7] V. V. Alexander *et al.*, "Power scalable 25 W supercontinuum laser from 2 to 2.5 µm with near-diffraction-limited beam and low output variability," *Opt. Lett.*, vol. 38, no. 13, pp. 2292–2294, 2013.

[8] C. W. Rudy, A. Marandi, K. L. Vodopyanov, and R. L. Byer, "Octave-spanning supercontinuum generation in in situ tapered As_2S_3 fiber pumped by a thulium-doped fiber laser," *Opt. Lett.*, vol. 38, no. 15, pp. 2865–2868, 2013.

[9] E. Sholokhov, A. Marakulin, A. Kurkov, and V. Tsvetkov, "All-fiber q-switched holmium laser," *Laser Phys. Lett.*, vol. 8, no. 5, pp. 382–385, 2011.

[10] A. Hemming, N. Simakov, J. Haub, and A. Carter, "A review of recent progress in holmium-doped silica fibre sources," *Opt. Fiber Technol.*, vol. 20, no. 6, pp. 621–630, 2014.

[11] N. Simakov *et al.*, "Holmium-doped fiber amplifier for optical communications at 2.05–2.13 µm," in *Proc. Opt. Fiber Commun. Conf.*, 2015, Paper Tu2C.6.

[12] N. Simakov, "Nikita Development of components and fibres for the power scaling of pulsed holmium-doped fibre sources," Ph.D. dissertation, 2017, p. 190.

[13] Y. Tang, X. Li, Z. Yan, X. Yu, Y. Zhang, and Q. J. Wang, "50-W 2 µm nanosecond all-fiber-based thulium-doped fiber amplifier," *IEEE J. Sel. Top. Quantum Electron.*, vol. 20, no. 5, pp. 537–543, Apr. 2014.

[14] A. Hemming *et al.*, "Pulsed operation of a resonantly pumped, linearly polarised, large mode area holmium-doped fibre amplifier," *Opt. Exp.*, vol. 22, no. 6, pp. 7186–7193, 2014.

[15] E. Lucas, L. Lombard, Y. Jaouën, S. Bordais, and G. Canat, "1 kW peak power, 110 ns single-frequency thulium doped fiber amplifier at 2050 nm," *Appl. Opt.*, vol. 53, no. 20, pp. 4413–4419, 2014.

[16] L. Li, B. Zhang, K. Yin, L. Yang, and J. Hou, "1 mJ nanosecond all-fiber thulium-doped fiber laser at 2.05 µm," *Opt. Exp.*, vol. 23, no. 14, pp. 18 098–18 105, 2015.

[17] A. Sincore, N. Bodnar, J. Bradford, A. Abdulfattah, L. Shah, and M. C. Richardson, "SBS threshold dependence on pulse duration in a 2053 nm single-mode fiber amplifier," *J. Lightw. Technol.*, vol. 35, no. 18, pp. 4000–4003, 2017.

[18] D. Lorenz, C. Romano, M. Eichhorn, and C. Kieleck, "Pulsed single-frequency polarization-maintaining holmium laser at 2050 & 2090 nm," *EPJ Web Conf.*, vol. 243, 2020, Art. no. 22001, doi: 10.1051/epjconf/202024322001.

[19] C. Romano, D. Lorenz, M. Eichhorn, and C. Kieleck, "kW class nanosecond polarization-maintaining holmium MOPA at 2050 nm and 2090 nm," in *Proc. OSA High-brightness Sources Light-driven Interact. Congr.*, 2020, Paper MF 2C.2.

[20] R. E. Tench, W. Walasik, and J.-M. Delavaux, "Novel highly efficient in-band pump wavelengths for medium slope efficiency holmium-doped fiber amplifiers," *J. Lightw. Technol.*, 2021, to be published, doi: 10.1109/JLT.2021.3067600.
[21] C. Giles, C. Burrus, D. DiGiovanni, N. Dutta, and G. Raybon, "Characterization of erbium-doped fibers and application to modeling 980-nm and 1480-nm pumped amplifiers," *IEEE Photon. Technol. Lett.*, vol. 3, no. 4, pp. 363–365, Apr. 1991.
[22] E. Desurvire, D. Bayart, B. Desthieux, and S. Bigo, *Erbium-Doped Fiber Amplifiers: Device and System Developments*, Wiley Series in Telecommunications and Signal Processing), Wiley, 2003.
[23] C. Giles and E. Desurvire, "Modeling erbium-doped fiber amplifiers," *J. Lightw. Technol.*, vol. 9, no. 2, pp. 271–283, 1991.
[24] C. Romano, Y. Jaouën, R. E. Tench, and J.-M. Delavaux, "Ultra-flat supercontinuum from 1.95 to 2.65 μm in a nanosecond pulsed thulium-doped fiber laser," *Opt. Fiber Technol.*, vol. 54, 2020, Art. no. 102113.
[25] G. Agrawal, *Nonlinear Fiber Optics*. Oxford, U.K.: Academic Press, 2013.
[26] J. del Valle-Hernandez, Y. O. Barmenkov, S. A. Kolpakov, J. L. Cruz, and M. V. Andres, "A distributed model for continuous-wave erbium-doped fiber laser," *Opt. Commun.*, vol. 284, no. 22, pp. 5342–5347, 2011.
[27] D. N. Schimpf, C. Ruchert, D. Nodop, J. Limpert, A. Tünnermann, and F. Salin, "Compensation of pulse-distortion in saturated laser amplifiers," *Opt. Exp.*, vol. 16, no. 22, pp. 17 637–17 646, Oct. 2008.
[28] D. Lin *et al.*, "Temporally and spatially shaped fully-fiberized ytterbium-doped pulsed MOPA," *Laser Phys. Lett.*, vol. 8, no. 10, pp. 747–753, 2011.
[29] G. Sobon, P. Kaczmarek, A. Antonczak, J. Sotor, A. Waz, and K. M. Abramski, "Pulsed dual-stage fiber MOPA source operating at 1550 nm with arbitrarily shaped output pulses," *Appl. Phys. B*, vol. 105, no. 4, pp. 721–727, 2011.
[30] H. Shi, F. Tan, Y. Cao, P. Wang, and P. Wang, "High-power diode-seeded thulium-doped fiber MOPA incorporating active pulse shaping," *Appl. Phys. B*, vol. 122, no. 10, p. 269, 2016.

158.91.143.166 on 2022-12-16 11:49:23